universe

MDPI

Article

Dark Matter in Fractional Gravity III: Dwarf Galaxies Kinematics

Francesco Benetti [1,2,*], Andrea Lapi [1,2,3,4], Giovanni Gandolfi [1,2,3], Minahil Adil Butt [1,2,3], Yacer Boumechta [1,2,3,5], Balakrishna S. Haridasu [1,2,3] and Carlo Baccigalupi [1,2,3]

1 Scuola Internazionale Superiore Studi Avanzati (SISSA), Physics Area, Via Bonomea 265, 34136 Trieste, Italy; lapi@sissa.it (A.L.); ggandolf@sissa.it (G.G.); mbutt@sissa.it (M.A.B.); yboumech@sissa.it (Y.B.); sandeep.haridasu@sissa.it (B.S.H.); bacci@sissa.it (C.B.)
2 Institute for Fundamental Physics of the Universe (IFPU), Via Beirut 2, 34014 Trieste, Italy
3 Istituto Nazionale Fisica Nucleare (INFN), Sezione di Trieste, Via Valerio 2, 34127 Trieste, Italy
4 Istituto di Radio-Astronomia (IRA-INAF), Via Gobetti 101, 40129 Bologna, Italy
5 ICTP-The Abdus Salam International Centre for Theoretical Physics, Strada Costiera 11, 34151 Trieste, Italy
* Correspondence: fbenetti@sissa.it

Abstract: Recently, we put forward a framework where the dark matter (DM) component within virialized halos is subject to a non-local interaction originated by fractional gravity (FG) effects. In previous works, we demonstrated that such a framework can substantially alleviate the small-scale issues of the standard ΛCDM paradigm, without altering the DM mass profile predicted by N-body simulations, and retaining its successes on large cosmological scales. In this paper, we investigate further, to probe FG via the high-quality data of individual dwarf galaxies, by exploiting the rotation velocity profiles inferred from stellar and gas kinematic measurements in eight dwarf irregulars, and the projected velocity dispersion profiles inferred from the observed dynamics of stellar tracers in seven dwarf spheroidals and in the ultra-diffuse galaxy DragonFly 44. We find that FG can reproduce extremely well the rotation and dispersion curves of the analyzed galaxies, performing in most instances significantly better than the standard Newtonian setup.

Keywords: dark matter; gravity; galaxy kinematics

Citation: Benetti, F.; Lapi, A.; Gandolfi, G.; Adil Butt, M.; Boumechta, Y.; Haridasu, B.S.; Baccigalupi, C. Dark Matter in Fractional Gravity III: Dwarf Galaxies Kinematics. *Universe* **2023**, *9*, 478. https://doi.org/10.3390/universe9110478

Academic Editor: Mauro D'Onofrio

Received: 16 October 2023
Revised: 2 November 2023
Accepted: 7 November 2023
Published: 8 November 2023

1. Introduction

The standard ΛCDM cosmology envisages galaxies to be hosted in virialized halos of dark matter (DM), which largely dominate the total mass and, hence, mostly determine the overall gravitational potential well and the dynamical properties of the baryons [1,2]. Remarkably, the density distribution of such halos is predicted by N-body simulations to follow an approximately universal shape, well described by the classic Navarro–Frenk–White [3] profile $\rho \propto (r/r_s)^{-1}\,(1+r/r_s)^{-2}$, with r_s being a characteristic scale radius where the logarithmic slope equals -2.

Only a minor deviation from such a scale-invariant behavior is expected, which amounts to a relationship between r_s and the total DM mass [4]. This is often expressed in terms of the concentration parameter $c_{200} \equiv R_{200}/r_s$, with R_{200} being the radius where the average DM density is 200 times that of a critical Universe $\rho_{\rm crit}$. In fact, recent zoom-in N-body simulations [5] have demonstrated that c_{200} correlates very well with the mass $M_{200} \equiv (4\pi/3)\,200\,\rho_{\rm crit}\,R_{200}^3$ over a remarkably extended range from $M_{200} \sim 10^{-5}\,M_\odot$ to $10^{15}\,M_\odot$.

Although on large scales observational data undoubtedly confirms the above picture, in the realm of dwarf galaxies with total masses $\lesssim 10^{11}\,M_\odot$ the situation becomes more uncertain. The most relevant issue for the present context emerges from galaxy kinematics and/or gravitational lensing data, which seem to indicate a much flatter density profile in the inner regions (i.e., a core), with respect to the cuspy NFW behavior; this occurrence is often referred to as the cusp–core problem [6–9].

In addition, there are other well-known issues associated with small galaxy scales that are worth mentioning [10]: the missing satellites problem [11,12] concerns the observed satellites in Milky-Way-sized galaxies that are found to be much less numerous than the bound DM halos in N-body simulations; the too-big-to-fail problem [13] concerns the halos hosting dwarf galaxies, which from kinematical measurements are found to be less massive than expected; the radial acceleration relation [14,15], the universal core surface density [16], and the core radius vs. the disk scale length scaling [17] all constitute tight empirical relationships between the properties of the DM and of the baryons that are extremely puzzling in the standard paradigm.

There are various viable solutions to these issues. The most obvious claims a misinterpretation of the data, due to poor resolution effects or other complex features in the DM distribution [18]. Another one invokes the impact of ordinary matter physics on the DM profile via stellar feedback [19,20] or transfer of energy/angular momentum to the DM via dynamical friction [21,22]. Another possibility involves nonstandard particle candidates, such as warm or sterile neutrino DM [23,24], fuzzy or particle-wave DM [25,26], self-interacting DM [27], and dark-photon DM [28,29], that by various processes (e.g., free streaming, quantum pressure effects, and/or dark sector interactions) can avoid the formation or later erase the inner cusp [30–32]. Finally, the observed galaxy kinematics can be explained with or without DM by modified gravity theories [33–35], such as MOND [36,37], fractional-dimensional gravity [38–42], and emergent entropic gravity [43,44].

Recently, in [45,46], we put forward a fractional gravity (FG) framework that strikes an intermediate course between a modified gravity theory and an exotic DM scenario (in this respect, similar to the dynamical non-minimally-coupled DM model explored by our team in [47–49]). FG envisages the DM component to be present though subject to a non-local interaction mediated by gravity. Specifically, in such a framework, the gravitational potential associated with a given DM density distribution (e.g., the NFW one) is determined by a modified Poisson equation including fractional derivatives (i.e., derivatives of noninteger type) that are aimed at describing non-locality. Very interestingly, it can be shown that FG can be reformulated in terms of the standard Poisson equation, but with an effective density distribution that is flatter in the inner region, with respect to the true one. This is actually the density behavior that an observer would infer by looking at the kinematic data and interpreting them in terms of standard Newtonian theory. Thus, in FG the cusp–core problem is basically solved at its root, as the cuspy NFW density profile of ΛCDM originates in FG a dynamic very similar to a cored profile in the standard Newtonian setting.

In [45,46] we tested FG over an extended mass range $M_{200} \sim 10^9$–$10^{15}\, M_\odot$ by exploiting stacked rotation curves of spiral galaxies and joint X-ray/Sunyaev-Zel'dovich observations of galaxy clusters. We found that FG performs extremely well in reproducing the data in all these systems. Moreover, our analysis highlighted that the strengths of FG effects tend to weaken toward more massive systems, thus implying that FG can substantially alleviate the small-scale issues of the standard ΛCDM paradigm, while retaining its successes on large cosmological scales.

For this paper, we aimed at investigating more deeply the regime where FG effects are expected to be more relevant, focusing on individual dwarf galaxies. In these objects, the cusp–core problem is observationally very pressing, and its solution via baryonic effects is difficult to be envisaged, given the paucity of baryons. Specifically, we probed FG, both in irregular dwarf (dwIrr) galaxies, by exploiting the rotation velocity profile inferred from stellar and gas kinematical measurements, and in dispersion-dominated dwarf spheroidals (dwSphs), by exploiting the velocity dispersion profile inferred from the dynamics of stellar tracers.

The structure of the paper is as follows: in Section 2, we describe our methods and data analysis; in Section 3, we present and discuss our results; in Section 4, we summarize our findings and outlook future perspectives. Throughout the work, we adopt the standard,

flat ΛCDM cosmology with rounded parameter values [50]: matter density $\Omega_m \approx 0.3$, baryon density $\Omega_b \approx 0.05$, and Hubble constant $H_0 = 100\,h$ km s^{-1} Mpc^{-1} with $h \approx 0.7$.

2. Methods

In this Section, we recall our basics framework, with particular focus on the basic kinematic observables in dwarfs. We then discuss the data and the Bayesian analysis exploited to probe such a scenario.

2.1. Dark Matter in Fractional Gravity

N-body simulations in the standard ΛCDM cosmology indicate that virialized halos of DM particles follow an approximately universal density profile, routinely described via the Navarro–Frenk–White [3] shape $\rho(r) = \rho_s\, r_s^3/r\,(r+r_s)^2$, in terms of a scale radius r_s and of a characteristic density ρ_s.

In the standard Newtonian theory, the potential $\Phi_{\rm N}(r)$ associated with a given density distribution $\rho(r)$ can be computed from the Poisson equation:

$$\Delta\Phi_{\rm N}(\mathbf{r}) = 4\pi G\,\rho(\mathbf{r}), \tag{1}$$

where Δ is the Laplacian operator; this is an inherently local equation, in that the potential at a point depends only on the value of the density there. For the spherically symmetric NFW profile, one easily finds that

$$\Phi_{\rm N}(r) = -\frac{GM_s}{r}\,\ln\!\left(1+\frac{r}{r_s}\right), \tag{2}$$

with $M_s \equiv 4\pi\,\rho_s\,r_s^3$. Computing the NFW mass $M(<r) = 4\pi\int_0^r {\rm d}r'\,r'^2\,\rho(r') = M_s\,[\ln(1+r/r_s) - r/(r+r_s)]$, it is easy to verify that $|{\rm d}\Phi_{\rm N}/{\rm d}r| = G\,M(<r)/r^2$, as a direct consequence of Birkhoff's theorem.

In the FG framework, the potential $\Phi_{\rm F}(r)$ is instead derived from the modified Poisson equation [40,45],

$$(-\Delta)^s\,\Phi_{\rm F}(\mathbf{r}) = -4\pi G\,\ell^{2-2s}\,\rho(\mathbf{r}), \tag{3}$$

where $(-\Delta)^s$ is the fractional Laplacian operator (see the excellent textbook [51] for details), $s \in [1, 3/2]$ is the fractional index (this range of values for s is required to avoid divergences; see Appendix A in [45]), and ℓ is a fractional length scale that must be introduced for dimensional reasons. At variance with the standard case, the fractional Laplacian is inherently nonlocal; the index s measures the strength of this nonlocality, while the length scale ℓ can be interpreted as the typical size below which gravitational effects are somewhat reduced and above which they are instead amplified by nonlocality.

In [45,46], ℓ was left as a free parameter to, be fitted by comparison with data. However, such a quantity enters only in the normalization of the potential but does not modify its radial shape; as such, it is strongly degenerate with the total mass, and very difficult to be constrained via pure kinematical data; essentially, one can only infer the combination $M_s\,\ell^{2-2s}$. Therefore, in the following, without loss of generality, we set it to $\ell \approx r_s$, which is the relevant spatial scale in the NFW density. This position is equivalent to making the original Poisson equation non-dimensional, in terms of quantities at r_s, and then fractionalized; this is a procedure often followed in the mathematical–physics literature [52–54], to insert fractional dynamics in a system, avoiding the addition of a dimensional parameter of ambiguous interpretation and problematic estimation.

For $s \in [1, 3/2)$, the solution reads [45]

$$\Phi_{\rm F}(r) = -\frac{GM_s}{r_s}\,\frac{1}{2^{2s}\sqrt{\pi}}\,\frac{\Gamma\left(\frac{3}{2}-s\right)}{\Gamma(s+1)}\,\frac{r_s}{r}\left\{\frac{2\pi s}{\sin(2\pi s)}\left[\left(1+\frac{r}{r_s}\right)^{2s-2}\right.\right.$$
$$\left.-\left(1-\frac{r}{r_s}\right)^{2s-2}\right] + \frac{(r/r_s)^{2s}}{1-(r/r_s)^2}\left[\left(1+\frac{r}{r_s}\right){}_2F_1\left(1,1,2s+1,\frac{r}{r_s}\right)\right. \tag{4}$$
$$\left.\left.+\left(1-\frac{r}{r_s}\right){}_2F_1\left(1,1,2s+1,-\frac{r}{r_s}\right)-\frac{4s}{2s-1}\right]\right\} \quad , \quad s \in [1,3/2),$$

with $\Gamma(s) = \int_0^\infty {\rm d}x\, x^{s-1}\, e^{-x}$ being the Euler Gamma function and ${}_2F_1(a,b,c;x) = \sum_{k=0}^\infty (a)_k\,(b)_k\,x^k/(c)_k\,k!$ being the ordinary hypergeometric function, in terms of the Pochammer symbols $(q)_k$ defined as $(q)_0 = 1$ and $(q)_k = q\,(q+1)\,\ldots\,(q+k-1)$; plainly, $\Phi_{\rm F}(r)$ for $s = 1$ coincides with the usual expression $\Phi_{\rm N}(r)$ of Equation (2). For the limiting case $s = 3/2$, the computation requires some principal value regularization, and the solution reads

$$\Phi_{\rm F}(r) = -\frac{G\,M_s}{r}\,\frac{1}{\pi}\left\{2\,\frac{r}{r_s}\left[\log\left(\frac{r}{r_s}\right)-1\right]-\left(1+\frac{r}{r_s}\right)\log\left(\frac{r}{r_s}\right)\log\left(1+\frac{r}{r_s}\right)\right.$$
$$\left.+\left(\frac{r}{r_s}-1\right){\rm Li}_2\left(1-\frac{r}{r_s}\right)-\left(1+\frac{r}{r_s}\right){\rm Li}_2\left(-\frac{r}{r_s}\right)+\frac{\pi^2}{6}\right\} \quad , \quad s = 3/2, \tag{5}$$

where ${\rm Li}_2(x) = \sum_{k=1}^\infty x^k/k^2$ is the dilogarithm function.

Being a nonlocal framework, in FG the Birkhoff theorem does not hold, but one can insist on writing $|{\rm d}\Phi_{\rm F}/{\rm d}r| = G\,M_F(<r)/r^2$, in terms of an effective mass $M_F(<r)$; then, one can differentiate the latter, to obtain an effective density profile $\rho_{\rm F}(r) = (1/4\pi\,r^2)\times {\rm d}M_{\rm F}/{\rm d}r$. These are actually the mass and density profiles that one would infer by looking at the dynamical observables and interpreting them in terms of Newtonian gravity. We illustrate the effective mass and density profiles for different values of s in Figure 1. With s increasing from unity (Newtonian case), the mass profile steepens and the density profile flattens; in the inner region, a uniform sphere behavior (corresponding to a cored density profile) tends to be progressively enforced.

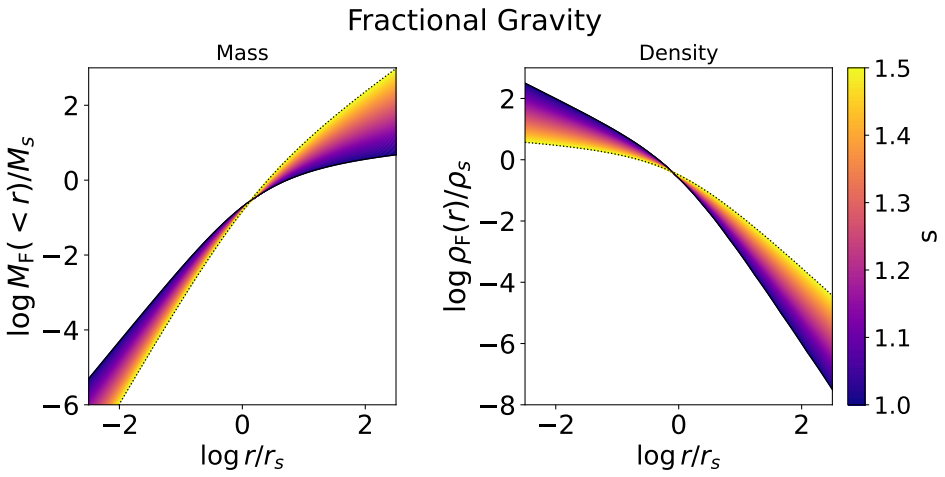

Figure 1. Radial profiles of effective mass (**left**) and density (**right**) in the FG framework for different values of the fractional index s (color-coded); for reference, the dotted lines refer to the maximal value $s = 3/2$.

These relevant profiles depend on the NFW scale radius r_s and density ρ_s or equivalently the mass $M_s = 4\pi\,\rho_s\,r_s^3$; however, in the following, it is convenient to trade off these quantities for the mass M_{200} and the concentration $c_{200} \equiv R_{200}/r_s$ at the reference radius R_{200}, where the average density is 200 times the critical density ρ_c. The conversion between these variables can be performed easily from the definition of R_{200} and from the NFW mass distribution. Furthermore, we adopt the relationship $c(M_{200}, z)$ in the ΛCDM cosmology derived from zoom-in N-body simulations by [5] and spanning twenty orders of magnitude in DM mass within the range $M_{200} \sim 10^{-5} - 10^{15}\,M_\odot$.

2.2. Dynamical Modeling

For a rotation-dominated system, the crucial quantity to be compared to the data is the total rotation velocity, which is given by

$$v_{\rm rot}^2(r) = v_{\rm halo}^2(r) + \frac{M_\star}{L}\,v_{\rm disk}^2(r) + v_{\rm gas}^2(r), \tag{6}$$

where $v_{\rm halo}^2 = G\,M_{\rm F}(<r)/r$ is the contribution from the DM halo, $v_{\rm gas}^2$ is the gas contribution from HI measurements, and $v_{\rm disk}^2$ is the contribution from the disk starlight appropriately converted into the stellar mass one via a global mass-to-light ratio $M_\star/L$. The overall rotation velocity depends on three parameters: namely, the stellar mass-to-light ratio $M_\star/L$, the total mass of the system M_{200}, and the fractional index s.

For a dispersion-dominated system, the crucial observable is the velocity dispersion projected along the line-of-sight (l.o.s.), which is given by [55,56]

$$\sigma_{\rm los}^2(R) = \frac{2}{\Sigma_\star(R)}\int_R^\infty {\rm d}r\left[1-\beta\,\frac{R^2}{r^2}\right]\frac{\rho_\star(r)\,\sigma_r^2(r)\,r}{\sqrt{r^2-R^2}}, \tag{7}$$

where $\beta \equiv 1 - \sigma_\theta^2/\sigma_r^2$ is the anisotropy parameter (hereafter assumed to be constant with the radius) and

$$\Sigma_\star(R) = 2\int_R^\infty {\rm d}r\,\frac{\rho_\star(r)\,r}{\sqrt{r^2-R^2}} \tag{8}$$

is the surface mass density of the tracers (e.g., stars), in terms of the volume one $\rho_\star(r)$; in addition, the radial velocity dispersion is obtained by solving the Jeans equation, which yields

$$\sigma_r^2(r) = \frac{1}{r^{2\beta}\,\rho_\star(r)}\int_r^\infty {\rm d}r'\,r'^{2\beta}\,\rho_\star(r')\,\frac{G\,[M_{\rm F}(<r') + M_\star(<r')]}{r'^2}, \tag{9}$$

in terms of the tracer mass $M_\star(<r) = 4\pi\int_0^r {\rm d}r'\,r'^2\,\rho_\star(r')$. Typically, for the dispersion-dominated galaxies considered in this work, stellar tracers are exploited, with a density distribution following the Plummer's [57] model (for DragonFly 44, we actually exploit a Sersic surface density profile, as detailed in [58]). A computationally efficient strategy to compute Equation (7) is detailed in Appendix A.

2.3. Data and Bayesian Analysis

We probed the FG framework by exploiting the rotation velocity profiles of dwIrr galaxies and the l.o.s. dispersion velocity profiles of dwSphs.

For rotation-dominated systems, we relied on the SPARC database [59,60], which provided the stellar and gas contribution to the rotation velocity, as found by numerically solving the standard Poisson equation for the observed surface brightness profile at 3.6 μm (with a reference stellar mass-to-light ratio $M_\star/L = 1$, so that this must be rescaled in building the total rotation velocity, as in Equation (6)), and the HI surface density profile. Specifically, we considered the 8 galaxies in SPARC that are classified as dwIrr and are flagged as having high-quality data on the rotation curve: D631-7, DDO64, DDO161, UGC731, UGC5005, UGC5414, UGC7608, and NGC3741. The latter is the galaxy with the

best dataset, and actually constitutes the object with the most extended rotation curve (relative to the half-light radius) measured to date.

For dispersion-dominated systems, we considered 7 Milky-Way dwSphs for which high-quality determination of the spatially-resolved dispersion velocity had been obtained via stellar tracers ([61,62]; see also, data collection by [63] and references therein) and for which tidal effects were not appreciably influencing the inner kinematics: Carina, Leo I, Leo II, Sculptor, Draco, Sextans, and Fornax. To these, we added the dispersion-dominated ultra-diffuse galaxy DragonFly 44 [58]. Note that ultra-diffuse galaxies are a mixed bag of objects with very different properties: some feature large angular momentum, a rich gas reservoir with ongoing active star-formation activity [64–67]; others show no signs of rotation, a poor gas content, and an old stellar population in passive evolution [58,68]. DragonFly 44 belongs to this last category and, being dispersion-dominated, was treated here along with the dwSph sample. In addition, it is a particularly interesting object, as it features a very small stellar mass, with respect to its large size; in fact, the DM mass is expected to dominate even at small radii. Therefore, DragonFly 44 has been exploited as a useful laboratory for testing the nature of DM and gravity [69,70].

In Table 1, we report some relevant properties of the galaxies considered in our analysis. Specifically, the first two columns list the circularized half-light radius of the projected surface brightness profile and the total luminosity, as determined from photometric observations (uncertainties are negligible for the purpose of this analysis); these quantities refer to the 3.6 μm band for dwIrr galaxies and to the V-band for dwSphs. The third column lists the stellar mass-to-light-ratio expected from stellar population synthesis models [71–73]: for disk-dominated dwIrr galaxy values, $M_\star/L \approx 0.5$ applies with few uncertainties at 3.6 μm; for dwSphs, the $M_\star/L$ values are estimated from the $V-I$ color index and thus are more dispersed and uncertain [63,69].

Table 1. Properties of the galaxy sample considered in this work: half-light radius, total luminosity, and mass-to-light ratio estimated from stellar population synthesis models (used in building the priors of our Bayesian analysis, see Section 2.3). The top half of the table includes rotation-dominated dwarfs, for which the listed quantities refer to the luminosity at 3.6 μm; the bottom half of the Table includes dispersion-dominated dwarfs, for which the listed quantities refer to the V-band luminosity.

Galaxy	$r_{1/2}$ **[kpc]**	$\log L\,[L_\odot]$	$M_\star/L\,[M_\odot/L_\odot]$
D631-7	1.22	8.28	0.5 ± 0.1
DDO64	1.22	8.18	0.5 ± 0.1
DDO161	2.04	8.74	0.5 ± 0.1
UGC731	1.40	8.51	0.5 ± 0.1
UGC5005	5.0	9.61	0.5 ± 0.1
UGC5414	2.33	9.05	0.5 ± 0.1
UGC7608	1.60	8.42	0.5 ± 0.1
NGC3741	0.32	7.45	0.5 ± 0.1
Carina	0.27	5.57	3.4 ± 2.9
Leo I	0.29	6.74	8.8 ± 5.6
Leo II	0.22	5.87	0.4 ± 0.4
Sculptor	0.31	6.36	3.6 ± 2.0
Draco	0.24	5.45	11.1 ± 4.7
Sextans	0.75	5.64	8.5 ± 3.3
Fornax	0.79	7.31	7.1 ± 6.0
DragonFly 44	3.87	8.37	1.5 ± 0.4

For our Bayesian analysis, we considered the parameter set $\theta \equiv (M_\star/L, M_{200}, s)$ for rotation-dominated dwarfs and $\theta \equiv (M_\star/L, \beta, M_{200}, s)$ for dispersion-dominated ones. To estimate these parameters, we adopted a Bayesian framework and built the Gaussian log-likelihood,

$$\log \mathcal{L}(\theta) = -\chi^2(\theta)/2\,, \tag{10}$$

where the chi-square $\chi^2(\theta) = \sum_i [\mathcal{M}(\theta, r_i) - \mathcal{D}(r_i)]^2 / \sigma^2_{\mathcal{D}}(r_i)$ was obtained by comparing our empirical model expectations $\mathcal{M}(\theta, r_i)$ to the data values $\mathcal{D}(r_i)$ with their uncertainties $\sigma_{\mathcal{D}}(r_i)$, summing over the different radial coordinates r_i of the data.

We adopted flat priors $\pi(\theta)$ on $s \in [1, 3/2]$ and on $\log M_{200}\,[M_\odot] \in [6, 13]$. Moreover, we assumed a lognormal prior on $\log M_\star/L$ with average and dispersion as expected from stellar population synthesis models (see Table 1). As to β, since by definition it varies in the range $(-\infty, 1]$, we actually preferred to perform inference on the symmetrized version $\beta_{\rm sym} \equiv \beta/(2-\beta)$ that mapped the original quantity in a compact domain $\beta_{\rm sym} \in (-1, 1]$; a flat prior on $\beta_{\rm sym}$ within this range was used. Finally, to help robustly break any possible degeneracy between the halo and stellar masses, we followed [60] and added as a ΛCDM prior the stellar mass vs. halo mass relation derived from multi-epoch abundance matching by [74], which was also consistent with independent observational determinations from satellite kinematics [75], rotation curve modeling [76], and weak lensing analysis [77].

We then sampled the parameter posterior distributions $\mathcal{P}(\theta) \propto \mathcal{L}(\theta)\,\pi(\theta)$ via the MCMC Python package `emcee` [78], running it with 10^4 steps and 100 walkers; each walker was initialized with a random position extracted from the priors discussed above. To speed up convergence, we adopted a mixture of differential evolution and snooker moves of the walkers, in proportions of 0.8 and 0.2, respectively, which emulated a parallel tempering algorithm. After checking the auto-correlation time, we removed the first 30% of the flattened chain, to ensure burn-in; the typical acceptance fractions of the various runs were around 30%.

3. Results

The results of our Bayesian analysis for rotation-dominated dwIrr galaxies are displayed in Figures 2 and 3 and in Table 2. Specifically, in the top panel of Figure 2, we illustrate the MCMC posterior distributions for two representative dwIrr galaxies in the sample: namely, NGC3741 (the one with the best and most extended data) and DDO64. The red lines/contours refer to the outcomes for FG, and the green ones to the outcomes for Newtonian gravity; the white crosses mark the best fit value of the parameters in FG. In the bottom panel, the best fit (solid lines) and the 2σ credible intervals (shaded areas) sampled from the posteriors are shown. The solid line is for the total rotation velocity, while the dashed and dotted lines show the halo and disk contribution, respectively; for comparison, the Newtonian best fit to the total velocity is reported in green. In Figure 3, the best fits in FG and in the Newtonian case are illustrated for the other six dwIrr galaxies in the sample. In Table 2, we summarize the marginalized posterior estimates of the parameters, both in FG and in the standard Newtonian case (marked with $s = 1$). The columns report the median values and the 1σ credible intervals of the stellar mass-to-light ratio $M_\star/L$, of the DM mass M_{200}, and of the fractional index s, the reduced χ^2_r of the fit, and the Bayesian inference criterion (BIC) for model comparison. The BIC is defined as $\mathrm{BIC} = 2\,\ln \mathcal{L}_{\rm max} + N_{\rm par}\,\ln N_{\rm data}$, in terms of the maximum likelihood estimate $\mathcal{L}_{\rm max}$ of the number of parameters $N_{\rm par}$ and the number of data points $N_{\rm data}$. The BIC comes from approximating the Bayes factor, which gives the posterior odds of one model against another, presuming that the models are equally favored a priori. Note that what matters is the relative value of the BIC among different models; in particular, a difference of around 10 or more indicates evidence in favor of the model with the smaller value.

The FG fits were always excellent, and comparable to or better than those in Newtonian gravity. In particular, for D631-7, DDO64, DDO161, UGC5005, UGC5414, and NGC3741, there was a clear preference for FG, both in terms of χ^2_r and of the BIC. In such cases, the fractional index took on typical values $s \approx 1.2$–1.3, the stellar mass-to-light ratios $M_\star/L$ were slightly larger than for the Newtonian case and more in line with the value around 0.5 expected from stellar population synthesis models, and the DM masses M_{200} were appreciably larger, by a few factors, than in the Newtonian fit. In the other cases, namely UGC731 and UGC7608, s was close to 1, the estimates of the fitting parameters in FG and in the Newtonian setting were consistent to within 1σ, and the overall quality of

the fits was comparable. We looked for some property of these two galaxies that could correlate with their smaller values of s, but were unable to reach a definite conclusion. Potentially interesting evidence came from the kinematics of their HI disks, which appeared asymmetric and disturbed by a past or ongoing gravitational interaction [79]; this could possibly have altered the shape of the outer rotation curve and originated a variant outcome when modeling it in the FG framework. An extended sample of a dwIrr galaxy with a high-quality rotation curve and environmental characterization would be needed, to investigate the issue further, in a statistically sound manner.

Table 2. Marginalized posterior estimates (mean and 1σ confidence intervals are reported) for the parameters from the MCMC analysis of the individual rotation-dominated dwIrr galaxies in fractional and Newtonian gravity (marked by $s = 1$). The columns report the values of the stellar mass-to-light ratio $M_\star/L$, of the DM mass M_{200}, of the fractional index s, of the reduced χ^2_r for the overall fit, and of the Bayesian inference criterion (BIC) for model comparison.

Galaxy	$\log M_\star/L$ $[M_\odot/L_\odot]$	$\log M_{200}$ $[M_\odot]$	s	χ^2_r	BIC
D631-7	$-0.39^{+0.07}_{-0.07}$	$10.59^{+0.06}_{-0.06}$	> 1.47	4.25	63
	$-0.77^{+0.07}_{-0.07}$	$10.15^{+0.03}_{-0.03}$	1	19.50	279
DDO64	$-0.28^{+0.09}_{-0.09}$	$10.55^{+0.07}_{-0.07}$	$1.16^{+0.04}_{-0.04}$	0.56	14
	$-0.45^{+0.08}_{-0.08}$	$10.36^{+0.06}_{-0.06}$	1	1.66	25
DDO161	$-0.76^{+0.07}_{-0.07}$	$10.26^{+0.03}_{-0.02}$	$1.35^{+0.02}_{-0.02}$	0.75	31
	$-0.82^{+0.06}_{-0.06}$	$10.44^{+0.01}_{-0.01}$	1	15.27	450
UGC731	$-0.26^{+0.08}_{-0.08}$	$10.70^{+0.03}_{-0.03}$	$1.05^{+0.02}_{-0.03}$	0.30	12
	$-0.29^{+0.08}_{-0.08}$	$10.67^{+0.02}_{-0.02}$	1	0.66	14
UGC5005	$-0.44^{+0.08}_{-0.08}$	$11.00^{+0.06}_{-0.06}$	$1.29^{+0.06}_{-0.06}$	0.64	15
	$-0.47^{+0.08}_{-0.08}$	$10.98^{+0.05}_{-0.05}$	1	3.13	35
UGC5414	$-0.28^{+0.09}_{-0.09}$	$10.91^{+0.07}_{-0.07}$	$1.28^{+0.04}_{-0.06}$	0.42	8
	$-0.67^{+0.07}_{-0.07}$	$10.54^{+0.04}_{-0.04}$	1	7.37	34
UGC7608	$-0.25^{+0.09}_{-0.09}$	$10.68^{+0.07}_{-0.07}$	$1.08^{+0.03}_{-0.06}$	1.26	14
	$-0.29^{+0.09}_{-0.09}$	$10.63^{+0.06}_{-0.06}$	1	1.35	14
NGC3741	$-0.21^{+0.08}_{-0.08}$	$10.29^{+0.04}_{-0.04}$	$1.23^{+0.03}_{-0.03}$	0.47	20
	$-0.49^{+0.07}_{-0.07}$	$10.09^{+0.02}_{-0.02}$	1	4.65	97

As can be seen in the top panel of Figure 2 for the representative cases of NGC3741 and DDO64, in FG there was no strong degeneracy in the fitting parameters, aside from a weak direct dependence between s and both $M_\star/L$ and M_{200}. The bottom panel of the same Figure shows that for NGC3741 and DDO64 the halo component largely dominated the rotation curve, with the baryonic contribution being relevant only in the innermost region within a few $r_{1/2}$; this situation was shared by all the dwIrr galaxies in the analyzed sample. Therefore, the shape of the rotation curve strongly constrains the halo mass/density profile; in particular, the rising trend of the rotation velocity out to large radii is difficult to be reproduced with an NFW profile in standard gravity, while the task can be easily achieved in the FG framework.

The results for dispersion-dominated galaxies are displayed in Figures 4 and 5 and in Table 3. Figure 4 focuses on the representative dwSph Sculptor and on the ultra-diffuse galaxy DragonFly 44. In the top panel of Figure 4, we illustrate the MCMC posterior distributions for Sculptor and DragonFly 44. As above, the red lines/contours refer to the outcomes for FG, the green ones to the outcomes for Newtonian gravity, with the white crosses marking the best fit value of the parameters in FG. In the bottom panel, the best fit (solid lines) and the 2σ credible intervals (shaded areas) sampled from the posteriors are shown, with the reference Newtonian fit in green. In Figure 5, the fits in FG and in the Newtonian case are illustrated for the other six dwSphs in the sample. In Table 3, we summarize the marginalized posterior estimates of the parameters for the dwSphs, both

in FG and in the standard Newtonian case (marked with $s = 1$). The columns report the median values and the 1σ credible intervals of the stellar mass-to-light ratio $M_\star/L$, of the symmetrized anisotropy parameter $\beta_{\rm sym}$, of the DM mass M_{200}, and of the fractional index s; the reduced χ^2_r of the fit and the BIC are also reported.

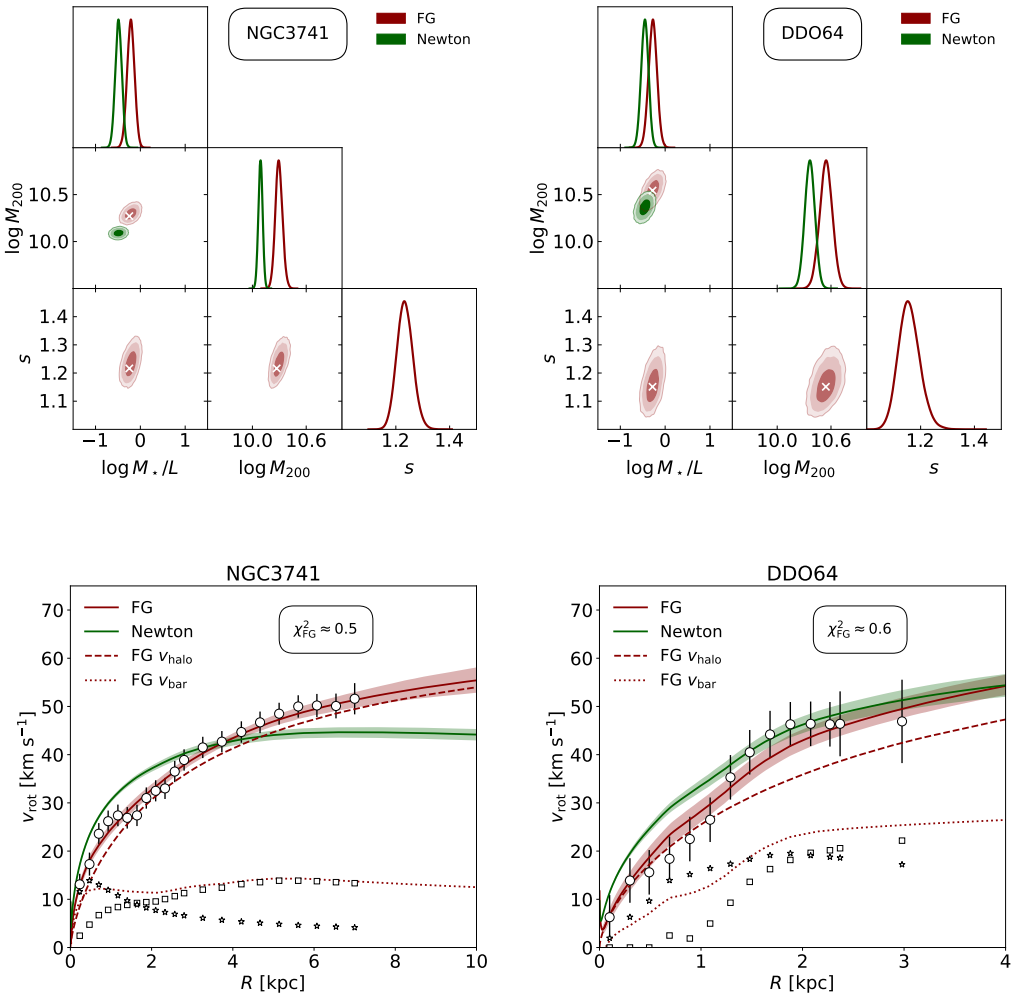

Figure 2. (**Top panel**): MCMC posterior distributions of the stellar mass-to-light ratio $M_\star/L$, the DM mass M_{200}, and the fractional index s for the galaxy NGC3741 (left) and DDO64 (right). The colored contours/lines refer to the standard Newtonian (green) and to the FG framework (red). The contours show 1–2–3σ confidence intervals, with the best fit values in FG identified by white crosses. The marginalized distributions are in arbitrary units (normalized to 1 at their maximum value). (**Bottom panel**): Fits to the rotation curve with the Newtonian (green) and the FG (red) framework for the galaxy NGC3741 (left) and DDO64 (right). The solid lines refer to the total rotation velocity, while (for clarity only in FG) the dashed line highlights the halo contribution and the dotted line the baryonic one. The solid lines illustrate the median, and the shaded areas show the 2σ credible interval from sampling the posterior distribution. The value of the reduced χ^2_r of the fit for FG is also reported. The circles represent data from the SPARC database [59] for the total rotation curve, while the contributions from the stellar (for $M_\star/L = 1$) and gaseous disks are highlighted by the starred and squared symbols, respectively.

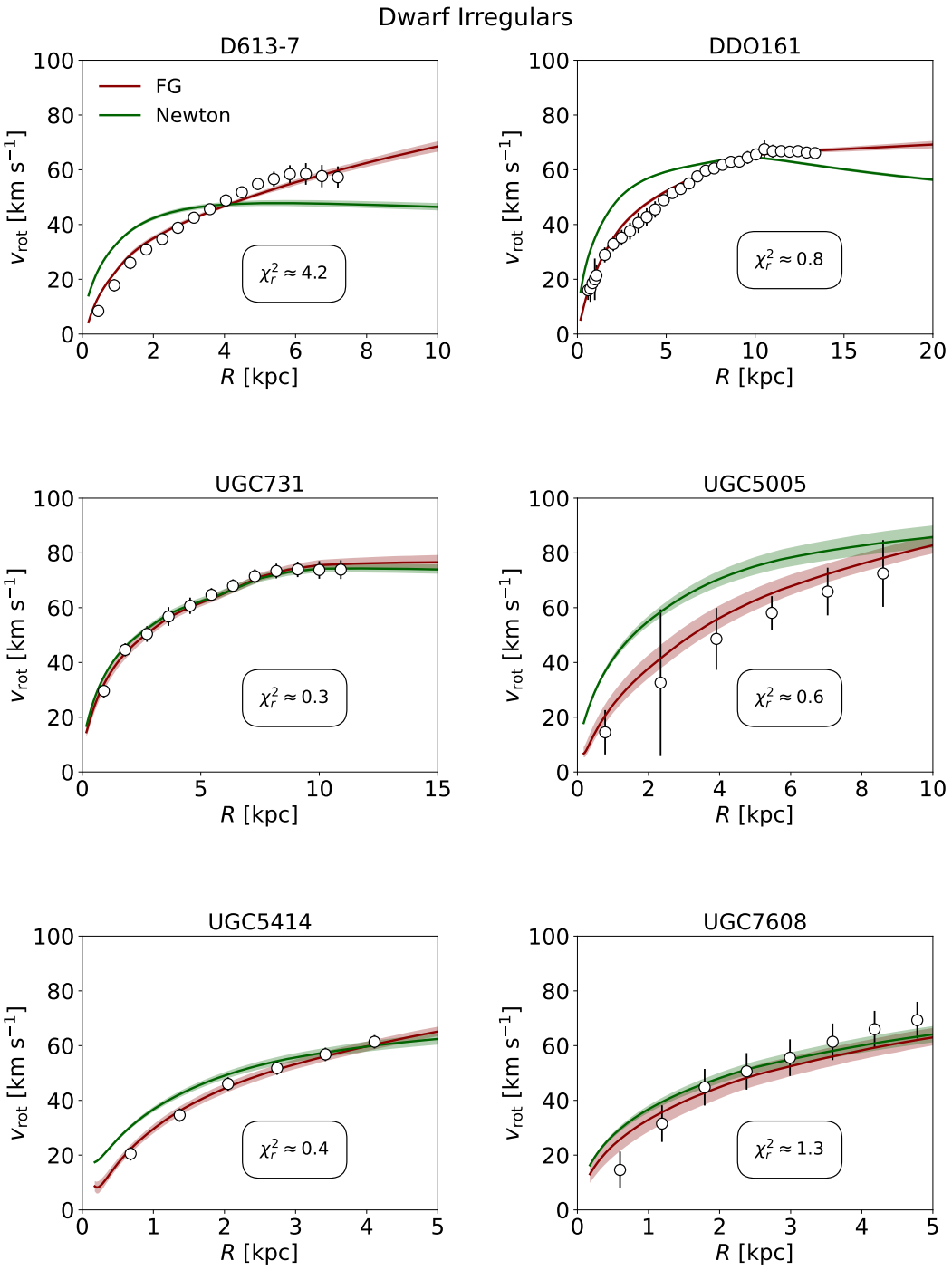

Figure 3. The same as the bottom panel in the previous figures for the other six dwIrr galaxies, as labeled. For clarity, data and models only for the total rotation curves are shown.

The FG fits to dispersion-dominated galaxies were very good, and in several instances appreciably better than in Newtonian gravity. In particular, for Carina, Leo I, Sculptor, and Sextans there was a clear preference for FG, both in terms of χ^2_r and in terms of the BIC. In such cases, the fractional index took on typical values $s \gtrsim 1.2$, the stellar mass-to-light ratios $M_\star/L$ were appreciably larger than for the Newtonian case and more in line with the prior from stellar population synthesis models, and the DM masses M_{200} were substantially larger by several factors, with respect to the Newtonian fits. In other cases, namely Leo II and Draco, the index $s \lesssim 1.1$ was smaller, the estimates of the fitting parameters in FG and in the Newtonian setting were consistent with 3σ, and the overall quality of the

fits was comparable. Finally, in the cases of Fornax and DragonFly 44 there was a clear preference for large values of $s \approx 1.5$, but the improvement in the FG fits with respect to the Newtonian case, while clear on a visual inspection, was not statistically significant enough to make definite conclusions.

As can be seen in the top panel of Figure 4 for Sculptor and DragonFly 44, the most relevant degeneracy between the fitting parameters involves s and the $\beta_{\rm sym}$, in such a way that FG models with larger s tend to be more isotropic. In fact, for Sculptor and DragonFly 44 the FG fit showed preference for almost isotropic orbits, while the Newtonian fit favored tangentially dominated motions. The bottom panel of the same Figure illustrates visually the quality of the FG fit for Sculptor and DragonFly 44, which was excellent within the scatter of the datapoints. FG performed definitively better than the Newtonian case for Sculptor, while for DragonFly 44 the evidence was rendered barely significant, in terms of reduced χ^2_r and of the BIC. In this respect, however, it is also interesting to look at the inset, where the excess kurtosis $\Delta\kappa$ is illustrated (the kurtosis is related to the fourth velocity moments of the stellar tracers, and the excess is with respect to the value 3 for a reference Gaussian velocity distribution). Although the measured value was largely uncertain, there was clearly a tendency towards a definite positive $\Delta\kappa$; qualitatively, this was consistent with the FG result at 2σ, while being highly discordant (more than 3σ) with the Newtonian fit. It is worth mentioning that the estimated $M_{200} \lesssim 10^{11}\, M_\odot$ from our analysis in FG is consistent with the recent determination from the abundance of globular clusters in DragonFly 44 by [80].

Table 3. Marginalized posterior estimates (mean and 1σ confidence intervals are reported) for the parameters from the MCMC analysis of the individual dispersion-dominated dwarf spheroidal in fractional (first lines) and Newtonian (second lines, with $s = 1$) gravity. The columns report the values of the stellar mass-to-light ratio $M_\star/L$, of the symmetrized anisotropy parameter $\beta_{\rm sym}$, of the DM mass M_{200}, of the fractional index s, of the reduced χ^2_r for the overall fit, and of the Bayesian inference criterion (BIC) for model comparison.

Galaxy	$\log M_\star/L$ $[M_\odot/L_\odot]$	$\beta_{\rm sym}$	$\log M_{200}$ $[M_\odot]$	s	χ^2_r	**BIC**
Carina	$+0.54^{+0.26}_{-0.26}$	$+0.19^{+0.11}_{-0.11}$	$9.77^{+0.12}_{-0.12}$	$1.37^{+0.04}_{-0.05}$	1.67	48
	$-0.75^{+0.28}_{-0.16}$	$-0.81^{+0.013}_{-0.12}$	$9.06^{+0.13}_{-0.06}$	1	3.49	87
Leo I	$+0.74^{+0.12}_{-0.07}$	$-0.08^{+0.16}_{-0.16}$	$10.35^{+0.08}_{-0.07}$	$1.37^{+0.11}_{-0.06}$	0.64	17
	$+0.19^{+0.16}_{-0.12}$	$-0.80^{+0.05}_{-0.07}$	$10.03^{+0.09}_{-0.07}$	1	2.64	39
Leo II	$-0.40^{+0.28}_{-0.28}$	$+0.37^{+0.25}_{-0.25}$	$9.50^{+0.13}_{-0.13}$	$1.11^{+0.04}_{-0.05}$	0.37	11
	$-0.74^{+0.24}_{-0.24}$	$+0.09^{+0.27}_{-0.27}$	$9.32^{+0.11}_{-0.11}$	1	0.42	9
Sculptor	$+0.60^{+0.19}_{-0.19}$	$-0.04^{+0.06}_{-0.06}$	$10.13^{+0.09}_{-0.09}$	$1.23^{+0.03}_{-0.05}$	1.32	54
	$-0.37^{+0.13}_{-0.13}$	$-0.32^{+0.06}_{-0.06}$	$9.51^{+0.06}_{-0.06}$	1	1.65	65
Draco	$+1.05^{+0.14}_{-0.14}$	$+0.01^{+0.17}_{-0.17}$	$9.93^{+0.09}_{-0.09}$	$1.13^{+0.03}_{-0.03}$	0.27	14
	$+0.75^{+0.12}_{-0.12}$	$-0.32^{+0.24}_{-0.17}$	$9.71^{+0.07}_{-0.07}$	1	0.56	15
Sextans	$+0.90^{+0.13}_{-0.13}$	$-0.34^{+0.07}_{-0.05}$	$9.94^{+0.08}_{-0.08}$	> 1.45	1.54	24
	$+0.54^{+0.12}_{-0.12}$	$-0.89^{+0.03}_{-0.07}$	$9.62^{+0.07}_{-0.07}$	1	3.07	38
Fornax	$-0.36^{+0.15}_{-0.12}$	$+0.16^{+0.03}_{-0.03}$	$10.03^{+0.1}_{-0.08}$	> 1.49	1.30	69
	< -1.84	$-0.16^{+0.04}_{-0.04}$	$9.08^{+0.03}_{-0.03}$	1	1.15	62
DragonFly 44	$+0.17^{+0.09}_{-0.09}$	$-0.12^{+0.11}_{-0.07}$	$10.79^{+0.07}_{-0.07}$	> 1.31	0.46	12
	$+0.09^{+0.09}_{-0.09}$	$-0.48^{+0.08}_{-0.08}$	$10.69^{+0.06}_{-0.06}$	1	1.27	16

By inspecting Tables 2 and 3, overall one can conclude that the evidence in favor of FG is less compelling in the dwSphs than in the dwIrr galaxies. This is for several reasons. First, the main observable for the dwIrr galaxies was the rotation velocity, which was a direct probe of the mass profile; contrariwise, in the dwSphs, the l.o.s. dispersion profile encased the mass profile in an integrated way, weighted by a kernel that depended on the tracer profiles and on the anisotropy parameter. In addition, the priors on the stellar

mass-to-light ratio from the population synthesis model were looser for the dwSphs than for the dwIrr galaxies (especially when considering 3.6 µm luminosities for the latter). Finally, the observed l.o.s. dispersion profiles were more scattered and featureless, with respect to the rotation curves. Thus, it should not be surprising that the constraints from the dwSphs were less statistically significant. Nevertheless, these systems may offer an environment where any evidence in favor of FG is more robust, as the lack of baryons even in the innermost regions does not allow us to rely on different interpretations related to baryonic-induced modification of the DM profile.

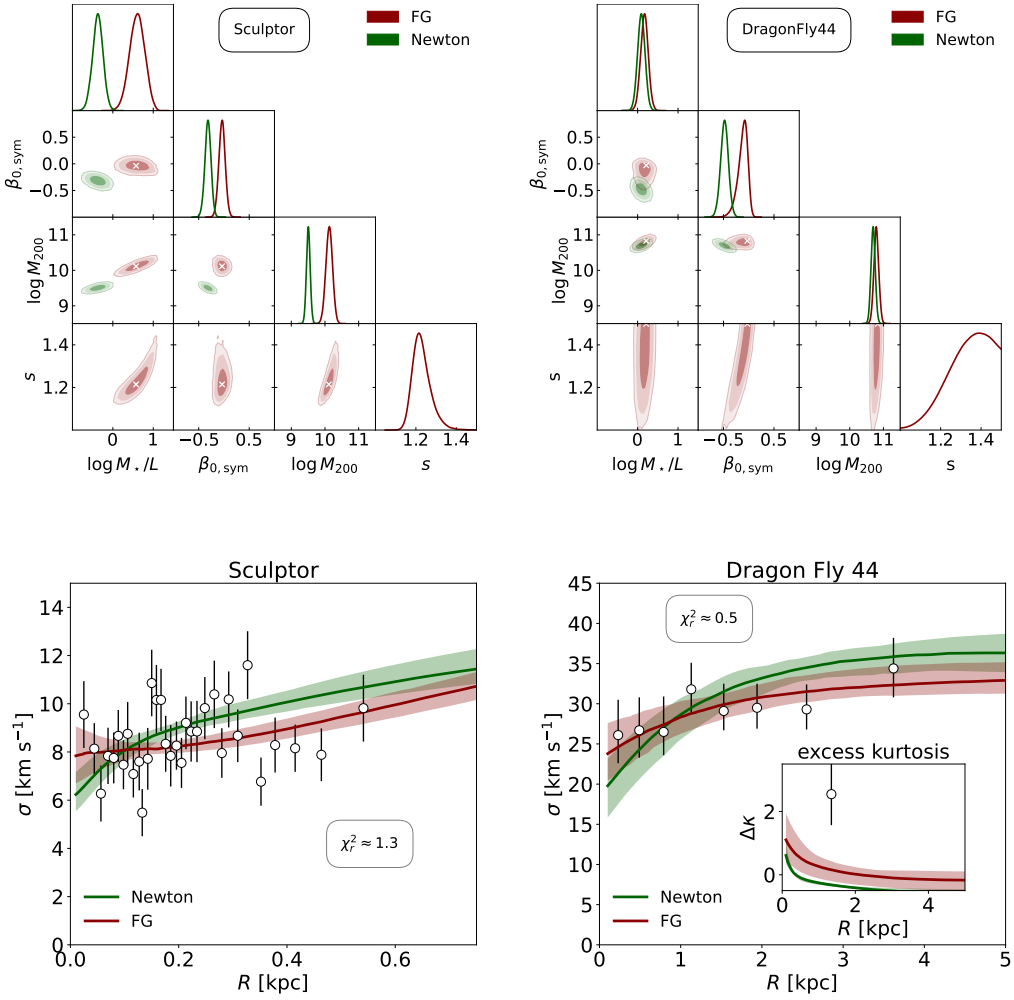

Figure 4. (**Top panel**): MCMC posterior distributions of the mass-to-light ratio $M_\star/L$, the symmetrized anisotropy parameter β_{sym}, the mass M_{200}, and the fractional index s for the dwSph galaxy Sculptor (left) and the ultra-diffuse galaxy DragonFly 44 (right). The colored contours/lines refer to the standard Newtonian (green) and to the FG framework (red). The contours show 1–2–3σ confidence intervals, with the best fit values in FG identified by white crosses. The marginalized distributions are in arbitrary units (normalized to 1 at their maximum value). (**Bottom panel**): Fits to the l.o.s. dispersion profile with the Newtonian (green) and the FG (red) framework for the dwSph galaxy Sculptor (left) and DragonFly 44 (right). The inset on the (**right bottom panel**) illustrates the excess kurtosis $\Delta\kappa$, with respect to a Gaussian velocity distribution. The solid lines illustrate the median, and the shaded areas show the 2σ credible interval from sampling the posterior distribution. The value of the reduced χ^2_r of the fit for FG is also reported. The circles represent data from [61] for Sculptor and from [58] for DragonFly 44.

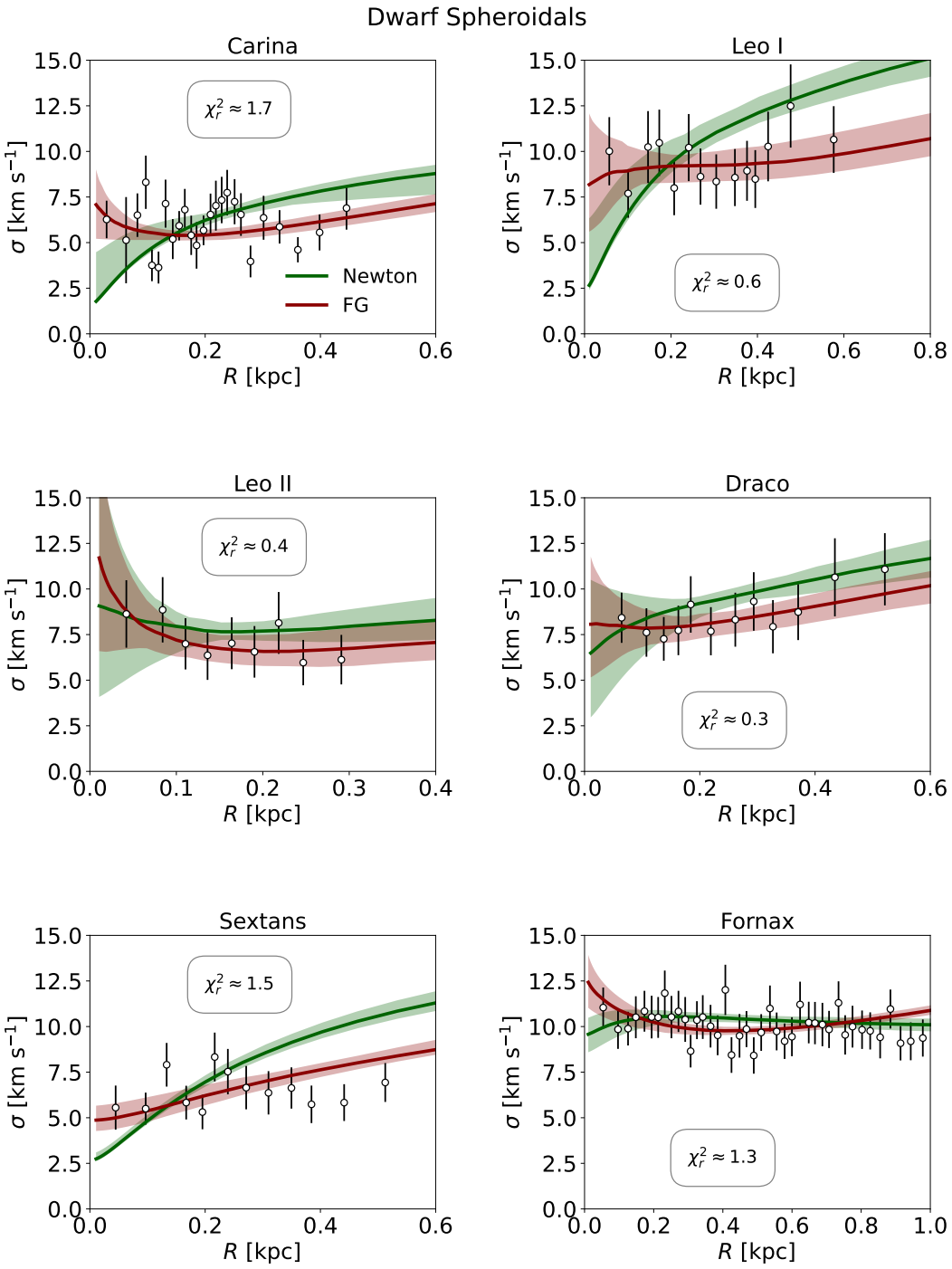

Figure 5. The same as the bottom panel in the previous figure for the six dwSph galaxies, as labeled.

Finally, in Figure 6 we illustrate two interesting scaling relations that constitute relevant crosschecks of our results. The diagram on the left panel displays the fractional index s as a function of the DM mass M_{200}. Apart from a few exceptions (objects with $s \lesssim 1.1$), the values from our analysis of individual dwarf galaxies in FG are consistent to within $2-3\sigma$ with the expectation from the relationship by [45] that was derived from fitting stacked rotation curves of rotation-dominated galaxies.

The diagram on the right reports the radial acceleration relation or RAR [14,15] between the total acceleration $g_{\rm tot}$ and the baryonic one $g_{\rm bar}$. This is an empirical relationship known to hold for different kind of galaxies, whose average and 1–2–3σ dispersion is plotted as an orange line surrounded by shaded areas. For rotationally supported systems, we computed $g_{\rm bar} = [v^2_{\rm gas}(r_{1/2}) + (M_\star/L) \times v^2_{\rm disk}(r_{1/2})]/r_{1/2}$ and $g_{\rm tot} = v^2_{\rm tot}(r_{1/2})/r_{1/2}$,

in terms of Equation (6). For dispersion-dominated systems, we instead estimated $g_{\rm bar} = G\,(M_\star/L) \times L_\star/2\,r_{1/2}^2$ and $g_{\rm tot} = 3\,\sigma_r^2(r_{1/2})/r_{1/2}$, in terms of Equation (9). For the sake of simplicity, we computed the accelerations at $r_{1/2}$ by using the best fit values of $M_\star/L$, M_{200}, and s from our analysis in FG. Reassuringly, almost all our estimated accelerations were consistent within $2-3\sigma$ with the RAR by [15], with the dwIrr galaxies clustering around the value of $g_{\rm bar}$ where the relation started to flatten, and with some dwSphs tracing the flat portion of the RAR and its scatter.

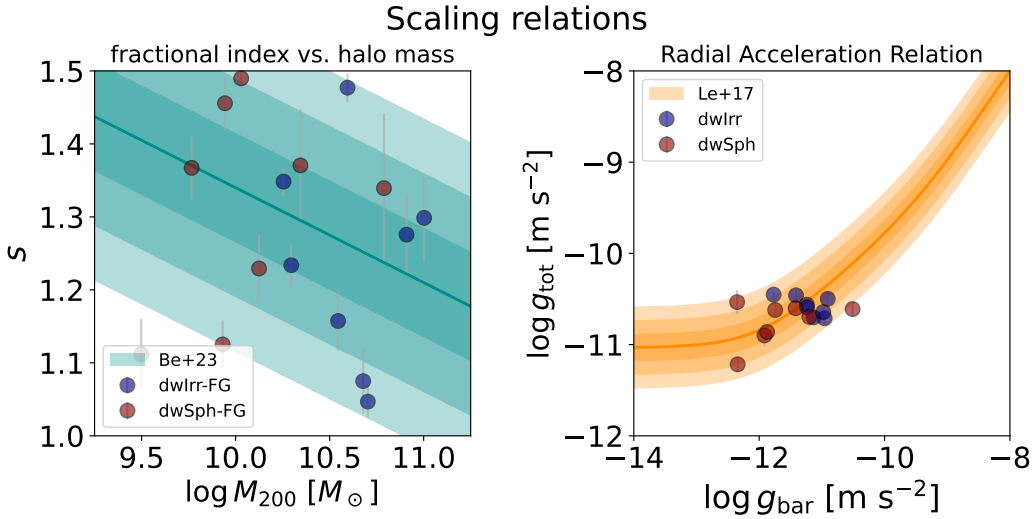

Figure 6. (**Left**) Fractional index as a function of DM mass from the outcomes of our Bayesian analysis. The blue circles refer to dwIrr galaxies and the red ones to dwSphs; the cyan line and shaded areas illustrate the best fit relation and 1–2–3σ dispersion from the analysis of stacked rotation curves for disk-dominated galaxies by [45]. (**Right**) The radial acceleration relation. The blue symbols refer to dwIrr galaxies and the red ones to dwSphs; the orange line and the shaded areas illustrate the best fit relation and 1–2–3σ dispersion from the determination by [15].

4. Summary

Dark matter (DM) in fractional gravity (FG) constitutes a framework that strikes an intermediate course between a modified gravity theory and an exotic DM scenario. It envisages the DM component in virialized cosmic structures to be affected by a non-local interaction mediated by gravity. Specifically, in such a framework the gravitational potential associated with a given DM density distribution is determined by a modified Poisson equation, including fractional derivatives, that are aimed at describing non-locality.

Remarkably, FG can be reformulated in terms of the standard Poisson equation, but with an effective density distribution that is flatter in the inner region, with respect to the true one. Therefore, FG offers a straightforward solution to the core–cusp problem of the standard ΛCDM model without altering the NFW density profile indicated by N-body simulations. An observer trying to interpret the kinematic data (e.g., rotation curves in dwIrr galaxies) in terms of the canonical (instead of the fractional) Poisson equation would claim the need for a cored density distribution. However, this is only apparent, as in FG the cuspy NFW density profile of ΛCDM originates a dynamic very similar to a cored profile in the standard Newtonian setting. In previous works [45,46], we tested our FG framework by exploiting stacked rotation curves of galaxies with different masses and joint X-ray/Sunyaev-Zel'dovich observations of galaxy clusters; our analysis highlighted that the strengths of FG effects tend to weaken toward more massive systems, so implying that dwarf galaxies constitute the best environment to constrain such a scenario.

In this paper, we investigated further, to probe FG via the high-quality data of individual dwarf galaxies, by exploiting the rotation velocity profiles inferred from stellar and gas kinematic measurements in eight dwarf irregulars, and the projected velocity dispersion profiles inferred from the observed dynamics of stellar tracers in seven dwarf spheroidals

and in the ultra-diffuse galaxy DragonFly 44. We found that FG reproduces extremely well the rotation and dispersion curves of all the analyzed galaxies, performing in most instances significantly better than the standard Newtonian gravity. With respect to the latter, the FG fits imply slightly larger stellar mass-to-light ratios $M_\star/L$ (more in line with the values expected from galaxy colors and stellar population synthesis models), appreciably larger DM masses M_{200} by a few factors, and (for dispersion-dominated systems) more isotropic orbits. We stressed that our best fit determinations of the fractional index s and of the DM masses M_{200} from the kinematics of individual dwarf galaxies are consistent to within 2–3σ with the relationship by [45] that was derived from fitting stacked rotation curves of rotation-dominated galaxies. We also highlighted that our findings are consistent with the radial acceleration relation by [15].

We pointed out that the evidence in favor of FG was less compelling for dwSphs than for dwIrr galaxies. This was for various reasons: the l.o.s. velocity dispersion was less sensitive than the rotation velocity to the mass profile; the uncertainties of the stellar mass-to-light ratio from stellar models (used as priors) were larger for the dwSphs than for the dwIrr galaxies; the uncertainty in dispersion profile measurements was larger than in the rotation curve data. However, it should be considered that dwSphs and ultra-diffuse galaxies could potentially provide a more robust environment to test FG, as they are strongly DM-dominated also in the innermost regions, and thus should not suffer from baryonic feedback processes or baryon-induced modification of the density profile. Future observations by astrometric space missions aimed at precision determination of the dispersion profiles in dwSphs and ultra-diffuse galaxies will be extremely helpful, to robustly strengthen the constraints on the FG framework presented here.

This work concludes a series of papers aimed at testing FG on different astrophysical scales, from dwarf galaxies to galaxy clusters. Overall, these have demonstrated that the FG framework can solve the small-scale issues of the standard ΛCDM, by reconciling with data the DM density distribution expected from N-body simulations, and saving its successes on large cosmological scales. Our future efforts will be directed at explaining the physical origin of the nonlocal effects subtended by the FG framework, and at investigating to what extent the theory can be generalized in a fully relativistic setting.

Author Contributions: Conceptualization, F.B., A.L. and G.G.; methodology, F.B., A.L. and G.G.; validation, M.A.B., Y.B., B.S.H. and C.B.; writing, A.L. All authors have read and agreed to the published version of the manuscript.

Funding: This work was partially funded from the projects: "Data Science methods for MultiMessenger Astrophysics & Multi-Survey Cosmology" funded by the Italian Ministry of University and Research, Programmazione triennale 2021/2023 (DM n.2503 dd. 9 December 2019), Programma Congiunto Scuole; EU H2020-MSCA-ITN-2019 n. 860744 *BiD4BESt: Big Data applications for black hole Evolution Studies*; PRIN MIUR 2017 prot. 20173ML3WW, *Opening the ALMA window on the cosmic evolution of gas, stars, and supermassive black holes*; Fondazione ICSC, Spoke 3 Astrophysics and Cosmos Observations; National Recovery and Resilience Plan (Piano Nazionale di Ripresa e Resilienza, PNRR) Project ID CN-00000013 "Italian Research Center on High-Performance Computing, Big Data and Quantum Computing" funded by MUR Missione 4 Componente 2 Investimento 1.4: Potenziamento strutture di ricerca e creazione di "campioni nazionali di R&S (M4C2-19)"— Next Generation EU (NGEU); INAF Large Grant 2022 funding scheme with the project *MeerKAT and LOFAR Team up: a Unique Radio Window on Galaxy/AGN co-Evolution*.

Data Availability Statement: Data are contained within the article.

Acknowledgments: We thank the anonymous referees for useful comments and suggestions. We acknowledge L. Danese, S. Liberati, and P. Salucci for helpful discussions.

Conflicts of Interest: The authors declare no conflicts of interest.

Appendix A. Projection Integrals

In this Appendix, we recall some useful formulas for the computation of the projection integrals involved in the analysis of Section 2. We start by considering the line-of-sight velocity dispersion of Equation (7):

$$\sigma^2_{\rm los}(R) = \frac{2}{\Sigma_\star(R)} \int_R^\infty {\rm d}r \left[1 - \beta \frac{R^2}{r^2}\right] \frac{\rho_\star(r)\, \sigma_r^2(r)\, r}{\sqrt{r^2 - R^2}}. \tag{A1}$$

Numerically computing the involved integral is rather challenging, as the integrand has a singularity in the lower limit of integration. To circumvent the issue, one can insert the explicit expression for σ_r from Equation (9) and obtain

$$\sigma^2_{\rm los}(R) = \frac{2}{\Sigma_\star(R)} \int_R^\infty {\rm d}r \left[1 - \beta \frac{R^2}{r^2}\right] \frac{r^{1-2\beta}}{\sqrt{r^2 - R^2}} \int_r^\infty {\rm d}s\, s^{2\beta-1}\, \rho_\star(s)\, v^2_{\rm rot}(s), \tag{A2}$$

where $v^2_{\rm rot}(r) \equiv G\,[M_{\rm F}(<r) + M_\star(<r)]/r$. It is now convenient to invert the order of integration, so that the double integral turns into

$$\sigma^2_{\rm los}(R) = \frac{2}{\Sigma_\star(R)} \int_R^\infty {\rm d}s\, s^{2\beta-1}\, \rho_\star(s)\, v^2_{\rm rot}(s) \int_R^s {\rm d}r \left[1 - \beta \frac{R^2}{r^2}\right] \frac{r^{1-2\beta}}{\sqrt{r^2 - R^2}} \tag{A3}$$

and the inner integral can be expressed in terms of special functions.

The overall results can be written as [81]

$$\sigma^2_{\rm los}(R) = \frac{2}{\Sigma_\star(R)} \int_R^\infty {\rm d}s\, \rho_\star(s)\, v^2_{\rm rot}(s)\, \mathcal{K}_2(s/R, \beta), \tag{A4}$$

in terms of the kernel

$$\mathcal{K}_2(x,\beta) = x^{2\beta-1} \left[-\frac{1}{2} B\left(\beta - \frac{1}{2}, \frac{1}{2}; \frac{1}{x^2}\right) + \frac{\beta}{2} B\left(\beta + \frac{1}{2}, \frac{1}{2}; \frac{1}{x^2}\right) + \right.$$
$$\left. + \frac{3-2\beta}{4} \frac{\sqrt{\pi}\,\Gamma(\beta - 1/2)}{\Gamma(\beta)}\right], \tag{A5}$$

where $\Gamma(a) = \int_0^\infty {\rm d}t\, t^{a-1}\, e^{-t}$ is the Gamma function and $B(a,b;x) \equiv \int_0^x {\rm d}t\, t^{a-1}\,(1-t)^{b-1}$ is the incomplete Beta function.

References

1. Rubin, V.C.; Ford, W.K., Jr.; Thonnard, N. Rotational properties of 21 Sc galaxies with a large range of luminosities and radii, from NGC 4605 ($R = 4$ kpc) to UGC 2885 ($R = 122$ kpc). *Astrophys. J.* **1996**, *281*, 27. [CrossRef]
2. Persic, M.; Salucci, P.; Stel, F. The universal rotation curve of spiral galaxies—I. The dark matter connection. *Mon. Not. R. Astron. Soc.* **1980**, *238*, 471.
3. Navarro, J.F.; Frenk, C.S.; White, S.D.M. A Universal Density Profile from Hierarchical Clustering. *Astrophys. J.* **1997**, *490*, 493. [CrossRef]
4. Dutton, A.A.; Maccio, A.V. Cold dark matter haloes in the Planck era: Evolution of structural parameters for Einasto and NFW profiles. *Mon. Not. R. Astron. Soc.* **2014**, *441*, 3359. [CrossRef]
5. Wang, J.; Bose, S.; Frenk, C. S.; Gao, L.; Jenkins, A.; Springel, V.; White, S.D.M. Universal structure of dark matter haloes over a mass range of 20 orders of magnitude. *Nature* **2020**, *585*, 39. [CrossRef]
6. Flores, R.A.; Primack, J.R. Observational and Theoretical Constraints on Singular Dark Matter Halos. *Astrophys. J.* **1994**, *427*, L1. [CrossRef]
7. Gentile, G.; Salucci, P.; Klein, U.; Vergani, D.; Kalberla, P. The cored distribution of dark matter in spiral galaxies. *Mon. Not. R. Astron. Soc.* **2004**, *351*, 903. [CrossRef]
8. de Blok, W.J.G.; Walter, F.; Brinks, E.; Trachternach, C.; Oh, S.-H.; Kennicutt, R.C., Jr. High-Resolution Rotation Curves and Galaxy Mass Models from THINGS. *Astron. J.* **2008**, *136*, 2648. [CrossRef]

9. Oh, S.-H.; Hunter, D.A.; Brinks, E.; Elmegreen, B.G.; Schruba, A.; Walter, F.; Rupen, M.P.; Young, L.M.; Simpson, C.E.; Johnson, M.C.; et al. High-resolution Mass Models of Dwarf Galaxies from LITTLE THINGS. *Astron. J.* **2015**, *149*, 1800. [CrossRef]
10. Bullock, J.S.; Boylan-Kolchin, M. Small-Scale Challenges to the ΛCDM Paradigm. *Ann. Rev. Astron. Astrophys.* **2017**, *55*, 343. [CrossRef]
11. Klypin, A.; Kravtsov, A.V.; Valenzuela, O.; Prada, F. Where Are the Missing Galactic Satellites? *Astrophys. J.* **1999**, *522*, 82. [CrossRef]
12. Moore, B.; Ghigna, S.; Governato, F.; Lake, G.; Quinn, T.; Stadel, J.; Tozzi, P. Dark Matter Substructure within Galactic Halos. *Astrophys. J.* **1999**, *524*, L19. [CrossRef]
13. Boylan-Kolchin, M.; Bullock, J.S.; Kaplinghat, M. The Milky Way's bright satellites as an apparent failure of ΛCDM. *Mon. Not. R. Astron. Soc.* **2012**, *422*, 1203. [CrossRef]
14. McGaugh, S.S.; Lelli, F.; Schombert, J.M. Radial Acceleration Relation in Rotationally Supported Galaxies. *Phys. Rev. Lett.* **2016**, *117*, 1101. [CrossRef] [PubMed]
15. Lelli, F.; McGaugh, S.S.; Schombert, J.M.; Pawlowski, M.S. One Law to Rule Them All: The Radial Acceleration Relation of Galaxies. *Astrophys. J.* **2017**, *836*, 152. [CrossRef]
16. Donato, F.; Gentile, G.; Salucci, P.; Frigerio Martins, C.; Wilkinson, M.I.; Gilmore, G.; Grebel, E.K.; Koch, A.; Wyse, R. A constant dark matter halo surface density in galaxies. *Mon. Not. R. Astron. Soc.* **2009**, *397*, 1169. [CrossRef]
17. Donato, F.; Gentile, G.; Salucci, P. Cores of dark matter haloes correlate with stellar scalelengths. *Mon. Not. R. Astron. Soc.* **2009**, *353*, L17. [CrossRef]
18. Oman, K.A.; Navarro, J.F.; Fattahi, A.; Frenk, C.S.; Sawala, T.; White, S.D.M.; Bower, R.; Crain, R.A.; Furlong, M.; Schaller, M.; et al. The unexpected diversity of dwarf galaxy rotation curves. *Mon. Not. R. Astron. Soc.* **2009**, *452*, 3650. [CrossRef]
19. Pontzen, A.; Governato, F. Cold dark matter heats up. *Nature* **2014**, *506*, 171. [CrossRef]
20. Freundlich, J.; Dekel, A.; Jiang, F.; Ishai, G.; Cornuault, N.; Lapiner, S.; Dutton, A.A.; Maccio, A.V. A model for core formation in dark matter haloes and ultra-diffuse galaxies by outflow episodes. *Mon. Not. R. Astron. Soc.* **2020**, *491*, 4253. [CrossRef]
21. El-Zant, A.; Shlosman, I.; Hoffman, Y. Dark Halos: The Flattening of the Density Cusp by Dynamical Friction. *Astrophys. J.* **2001**, *560*, 636. [CrossRef]
22. Tonini, C.; Lapi, A.; Salucci, P. Angular Momentum Transfer in Dark Matter Halos: Erasing the Cusp. *Astrophys. J.* **2006**, *649*, 591. [CrossRef]
23. Bode, P.; Ostriker, J.P.; Turok, N. Halo Formation in Warm Dark Matter Models. *Astrophys. J.* **2001**, *556*, 93. [CrossRef]
24. Lovell, M.; Frenk, C.S.; Eke, V.R.; Jenkins, A.; Gao, L.; Theuns, T. The properties of warm dark matter haloes. *Mon. Not. R. Astron. Soc.* **2014**, *439*, 300. [CrossRef]
25. Hu, W.; Barkana, R.; Gruzinov, A. Fuzzy Cold Dark Matter: The Wave Properties of Ultralight Particles. *Phys. Rev. Lett.* **2000**, *85*, 1158. [CrossRef]
26. Hui, L.; Ostriker, J.P.; Tremaine, S.; Witten, E. Ultralight scalars as cosmological dark matter. *Phys. Rev. D* **2017**, *95*, 3541. [CrossRef]
27. Vogelsberger, M.; Zavala, J.; Cyr-Racine, F.-Y.; Pfrommer, C.; Bringmann, T.; Sigurdson, K. ETHOS-An effective theory of structure formation: Dark matter physics as a possible explanation of the small-scale CDM problems. *Mon. Not. R. Astron. Soc.* **2016**, *460*, 1399. [CrossRef]
28. McDermott, S.D.; Witte, S.J. Cosmological evolution of light dark photon dark matter. *Phys. Rev. D* **2020**, *101*, 3030. [CrossRef]
29. Bolton, J.S.; Caputo, A.; Liu, H.; Viel, M. Comparison of Low-Redshift Lyman-α Forest Observations to Hydrodynamical Simulations with Dark Photon Dark Matter. *Phys. Rev. Lett.* **2022**, *129*, 1102. [CrossRef]
30. Bertone, G.; Hooper, D.; Silk, J. Particle dark matter: Evidence, candidates and constraints. *Phys. Rev.* **2004**, *405*, 279. [CrossRef]
31. Adhikari, R.; Agostini, M.; Ky, N.A.; Araki, T.; Archidiacono, M.; Bahr, M.; Baur, J.; Behrens, J.; Bezrukov, F.; Bhupal Dev, P. S.; et al. A White Paper on keV sterile neutrino Dark Matter. *Journ. Cosmol. Astropart. Phys.* **2017**, *1*, 25. [CrossRef]
32. Salucci, P.; Esposito, G.; Lambiase, G.; Battista, E.; Benetti, M.; Bini, D.; Boco, L.; Sharma, G.; Bozza, V.; Buoninfante, L.; et al. Einstein, Planck and Vera Rubin: Relevant encounters between the Cosmological and the Quantum Worlds. *Front. Phys.* **2021**, *8*, 603190. [CrossRef]
33. Clifton, T.; Ferreira, P.G.; Padilla, A.; Skordis, C. Modified gravity and cosmology. *Phys. Rep.* **2012**, *513*, 1–189. [CrossRef]
34. Nojiri, S.; Odintsov, S.D.; Oikonomou, V.K. Modified gravity theories on a nutshell: Inflation, bounce and late-time evolution. *Phys. Rep.* **2017**, *692*, 1–104. [CrossRef]
35. Saridakis, E.N.; Lazkoz, R.; Salzano, V.; Moniz, P.V.; Capozziello, S; Beltran J.J.; De Laurentis, M.; Olmo, G.J. *Modified Gravity and Cosmology: An Update by the CANTATA Network*; Springer International Publishing: Cham, Switzerland, 2021; ISBN 978-3-030-83715-0.
36. Milgrom, M. A modification of the Newtonian dynamics as a possible alternative to the hidden mass hypothesis. *Astrophys. J.* **2017**, *270*, 365. [CrossRef]
37. Famaey, B.; McGaugh, S.S. Modified Newtonian Dynamics (MOND): Observational Phenomenology and Relativistic Extensions. *Liv. Rev. Relat.* **2012**, *15*, 10. [CrossRef]
38. Varieschi, G.U. Newtonian Fractional-Dimension Gravity and MOND. *Found. Phys.* **2020**, *50*, 1608. [CrossRef]
39. Varieschi, G.U. Newtonian fractional-dimension gravity and rotationally supported galaxies. *Mon. Not. R. Astron. Soc.* **2021**, *503*, 1915. [CrossRef]
40. Giusti, A. MOND-like fractional Laplacian theory. *Phys. Rev. D* **2020**, *101*, 124029. [CrossRef]

41. Giusti, A.; Garrappa, R.; Vachon, G. On the Kuzmin model in fractional Newtonian gravity. *EPJP* **2020**, *135*, 798. [CrossRef]
42. Calcagni, G.; Varieschi, G.U. Gravitational potential and galaxy rotation curves in multi-fractional spacetimes. *J. High Energy Phys.* **2022**, *8*, 24. [CrossRef]
43. Verlinde, E.P. Emergent Gravity and the Dark Universe. *Sci. Post. Phys.* **2017**, *2*, 16. [CrossRef]
44. Yoon, Y.; Park, J.-C.; Hwang, H.S. Understanding galaxy rotation curves with Verlinde's emergent gravity. *Class. Quant. Grav.* **2023**, *40*, 02LT01. [CrossRef]
45. Benetti, F.; Lapi, A.; Gandolfi, G.; Salucci, P.; Danese, L. Dark Matter in Fractional Gravity I: Astrophysical Tests on Galactic Scales. *Astrophys. J.* **2023**, *949*, 65. [CrossRef]
46. Benetti, F.; Lapi, A.; Gandolfi, G.; Haridasu, B.S.; Danese, L. Dark Matter in Fractional Gravity II: Tests in Galaxy Clusters. *Universe* **2023**, *9*, 329. [CrossRef]
47. Gandolfi, G.; Lapi, A.; Liberati, S. Self-gravitating Equilibria of Non-minimally Coupled Dark Matter Halos. *Astrophys. J.* **2021**, *910*, 76. [CrossRef]
48. Gandolfi, G.; Lapi, A.; Liberati, S. Empirical Evidence of Nonminimally Coupled Dark Matter in the Dynamics of Local Spiral Galaxies? *Astrophys. J.* **2022**, *929*, 48. [CrossRef]
49. Gandolfi, G.; Haridasu, B.S.; Liberati, S.; Lapi, A. Looking for Traces of Non-minimally Coupled Dark Matter in the X-COP Galaxy Clusters Sample. *Astrophys. J.* **2023**, *952*, 105. [CrossRef]
50. Aghanim, N.; Akrami, Y.; Ashdown, M.; Aumont, J.; Baccigalupi, C.; Ballardini, M.; Banday, A.J.; Barreiro, R.B.; Bartolo, N.; Basak, S.; et al. [Planck Collaboration]. Planck 2018 results. VI. Cosmological parameters. *Astron. Astrophys.* **2020**, *641*, A6.
51. Uchaikin, V.V. *Fractional Derivatives for Physicists and Engineers: Background and Theory*; Nonlinear Physical Science, Higher Education Press: Beijing, China; Springer: Berlin/Heidelberg, Germany, 2013; ISBN 978-3-642-33910-3.
52. Gomez-Aguilar, J.F.; Rosales-Garcıa, J.J.; Bernal-Alvarado, J.J.; Cordova-Fraga, T; Guzman-Cabrera, R. Fractional mechanical oscillators. *Riv. Mex. Phys.* **2012**, *58*, 348.
53. Ebaid, A.; El-Zahar, E.R.; Aljohani, A.F.; Salah, B.; Krid, M.; Tenreiro Machado, J. Analysis of the two-dimensional fractional projectile motion in view of the experimental data. *Nonlin. Dynam.* **2019**, *97*, 1711. [CrossRef]
54. Pranjivan Mehta, P.; Pang, G.; Song, F.; Em Karniadakis, G. Discovering a Universal Variable-Order Fractional Model for Turbulent Couette Flow Using a Physics-informed Neural Network. *Fract. Calc. Appl. Analys.* **2019**, *22*, 6.
55. Binney, J. Dynamics of elliptical galaxies and other spheroidal components. *Ann. Rev. Astron. Astrophys.* **1982**, *20*, 399. [CrossRef]
56. Lokas, E.L.; Mamon, G.A. Properties of spherical galaxies and clusters with an NFW density profiles. *Mon. Not. R. Astron. Soc.* **2001**, *321*, 155. [CrossRef]
57. Plummer, H. C. On the problem of distribution in globular star clusters. *Mon. Not. R. Astron. Soc.* **2001**, *71*, 460. [CrossRef]
58. van Dokkum, P.; Wasserman, A.; Danieli, S.; Abraham, R.; Brodie, J.; Conroy, C.; Forbes, D.A.; Martin, C.; Matuszewski, M.; Romanowsky, A.J.; et al. Spatially Resolved Stellar Kinematics of the Ultra-diffuse Galaxy Dragonfly 44. I. Observations, Kinematics, and Cold Dark Matter Halo Fits. *Astrophys. J.* **2019**, *880*, 91. [CrossRef]
59. Lelli, F.; McGaugh, S.S.; Schombert, J.M. SPARC: Mass Models for 175 Disk Galaxies with Spitzer Photometry and Accurate Rotation Curves. *Astron. J.* **2016**, *152*, 157. [CrossRef]
60. Li, P.; Lelli, F.; McGaugh, S.; Schombert, J. A Comprehensive Catalog of Dark Matter Halo Models for SPARC Galaxies. *Astrophys. J. Suppl. Ser.* **2020**, *247*, 31. [CrossRef]
61. Walker, M.G.; Mateo, M.; Olszewski, E.W. Stellar Velocities in the Carina, Fornax, Sculptor, and Sextans dSph Galaxies: Data From the Magellan/MMFS Survey. *Astron. J.* **2009**, *137*, 3100. [CrossRef]
62. Mateo, M.; Olszewski, E.W.; Walker, M.G. The Velocity Dispersion Profile of the Remote Dwarf Spheroidal Galaxy Leo I: A Tidal Hit and Run?. *Astrophys. J.* **2009**, *675*, 201. [CrossRef]
63. de Martino, I.; Diaferio, A.; Ostorero, L. Dynamics of dwarf galaxies in $f(R)$ gravity. *Mon. Not. R. Astron. Soc.* **2023**, *519*, 4424. [CrossRef]
64. Leisman, L.; Haynes, M.P.; Janowiecki, S.; Hallenbeck, G.; Jozsa, G.; Giovanelli, R.; Adams, E.A.K.; Bernal Neira, D.; Cannon, J.M.; Janesh, W.F.; et al. (Almost) Dark Galaxies in the ALFALFA Survey: Isolated H I-bearing Ultra-diffuse Galaxies. *Astrophys. J.* **2017**, *842*, 133. [CrossRef]
65. Mancera Pina, P.E.; Fraternali, F.; Oman, K.A.; Adams, E.A.K.; Bacchini, C.; Marasco, A.; Oosterloo, T.; Pezzulli, G.; Posti, L.; Leisman, L.; et al. Robust H I kinematics of gas-rich ultra-diffuse galaxies: Hints of a weak-feedback formation scenario. *Mon. Not. R. Astron. Soc.* **2020**, *495*, 3636. [CrossRef]
66. Mancera Piña, P.E.; Aguerri, J.A.L.; Peletier, R.F.; Venhola, A.; Trager, S.; Choque Challapa, N. The evolution of ultra-diffuse galaxies in nearby galaxy clusters from the Kapteyn IAC WEAVE INT Clusters Survey. *Mon. Not. R. Astron. Soc.* **2019**, *485*, 1036. [CrossRef]
67. Sengupta, C.; Scott, T. C.; Chung, A.; Wong, O. I. Dark matter and H I in ultra-diffuse galaxy UGC 2162. *Mon. Not. R. Astron. Soc.* **2019**, *488*, 3222. [CrossRef]
68. van Dokkum, P.G.; Abraham, R.; Merritt, A.; Zhang, J.; Geha, M.; Conroy, C. Forty-seven Milky Way-sized, Extremely Diffuse Galaxies in the Coma Cluster. *Astrophys. J.* **2015**, *798*, L45. [CrossRef]
69. Wasserman, A.; van Dokkum, P.; Romanowsky, A.J.; Brodie, J.; Danieli, S.; Forbes, D.A.; Abraham, R.; Martin, C.; Matuszewski, M.; Villaume, A.; et al. Spatially Resolved Stellar Kinematics of the Ultra-diffuse Galaxy Dragonfly 44. II. Constraints on Fuzzy Dark Matter. *Astrophys. J.* **2019**, *885*, 155. [CrossRef]

70. Julio, M.P.; Brinchmann, J.; Zoutendijk, S.L.; Read, J.I.; Vaz, D.; Kamann, S.; Krajnovic, D.; Boogaard, L.A.; Steinmetz, M.; Bouche, N. The MUSE-Faint survey. V. Constraining Scalar Field Dark Matter with Antlia B. *Astron. Astrophys.* **2023**, 678, A38 [CrossRef]
71. Bell, E.F.; de Jong, R.S. Stellar Mass-to-Light Ratios and the Tully-Fisher Relation. *Astrophys. J.* **2001**, *550*, 212. [CrossRef]
72. Portinari, L.; Sommer-Larsen, J.; Tantalo, R. On the mass-to-light ratio and the initial mass function in disc galaxies. *Mon. Not. R. Astron. Soc.* **2004**, *346*,691. [CrossRef]
73. Schombert, J. McGaugh, S. Lelli, F. The mass-to-light ratios and the star formation histories of disc galaxies. *Mon. Not. R. Astron. Soc.* **2019**, *483*, 1496.
74. Moster, B.P.; Naab, T.; White, S.D.M. Galactic star formation and accretion histories from matching galaxies to dark matter haloes. *Mon. Not. R. Astron. Soc.* **2013**, *428*, 3121. [CrossRef]
75. Lange, J.U.; van den Bosch, F.C.; Zentner, A.R.; Wang, K.; Villarreal, A.S. Updated results on the galaxy-halo connection from satellite kinematics in SDSS. *Mon. Not. R. Astron. Soc.* **2019**, *487*, 3112. [CrossRef]
76. Lapi, A.; Salucci, P.; Danese, L. Precision Scaling Relations for Disk Galaxies in the Local Universe. *Astrophys. J.* **2018**, *859*, 2. [CrossRef]
77. Mandelbaum, R.; Wang, W.; Zu, Y.; White, S.; Henriques, B.; More, S. Strong bimodality in the host halo mass of central galaxies from galaxy-galaxy lensing. *Mon. Not. R. Astron. Soc.* **2016**, *457*, 3002. [CrossRef]
78. Foreman-Mackey, D.; Hogg, D.W.; Lang, D.; Goodman, J. emcee: The MCMC Hammer. *Publ. Astron. Soc. Pac.* **2013**, *125*, 306. [CrossRef]
79. Swaters, R. A.; van Albada, T. S.; van der Hulst, J. M.; Sancisi, R. The Westerbork HI survey of spiral and irregular galaxies. I. HI imaging of late-type dwarf galaxies. *Astron. Astrophys.* **2002**, *390*, 829. [CrossRef]
80. Saifollahi, T.; Trujillo, I.; Beasley, M.A.; Peletier, R.F.; Knapen, J.H. The number of globular clusters around the iconic UDG DF44 is as expected for dwarf galaxies. *Mon. Not. R. Astron. Soc.* **2019**, *502*, 5921. [CrossRef]
81. Mamon, G.A.; Lokas, E. L. Dark matter in elliptical galaxies—II. Estimating the mass within the virial radius. *Mon. Not. R. Astron. Soc.* **2016**, *363*, 705. [CrossRef]